

# Monitoring micro-failures prior to granular avalanches using Diffusive Acoustic Wave Spectroscopy and Grain Tracking

Ibrahim Awada<sup>1</sup>, Michel Bornert<sup>1</sup>, Vincent Langlois<sup>1</sup>, and Julien Léopoldès<sup>1,\*</sup>

<sup>1</sup>Navier, Ecole des Ponts, Univ. Gustave Eiffel, CNRS, Marne-la-Vallée 77420, France

**Abstract.** Granular avalanches occur in both natural and industrial environments, influencing landscape evolution and posing risks in engineering applications. Understanding their precursors is crucial for predicting failure events and mitigating hazards. This study explores kinematic indicators of impending avalanches through strain fluctuations, measured via Diffusive Acoustic Wave Spectroscopy and grain tracking. We find that strain fluctuations grow exponentially as the system approaches the avalanche angle, and that the amplitude of this growth is controlled by the initial packing fraction of the pile.

## 1 Introduction

Granular materials, such as sand, snow, and debris, exhibit complex behaviors under stress, including gradual deformation and sudden failure in the form of avalanches. The study of granular avalanches is relevant in geophysics, civil engineering, and industrial processing [1, 2]. Predicting these events requires identifying early-stage instabilities, which manifest as microstructural changes, stress redistributions, and slope adjustments [3].

A key aspect of avalanche prediction is finding mechanical indicators of system instability [4]. Experimental studies have detected signals preceding avalanches manifesting as stress propagation patterns [5] or variation of the wave speed [6] that indicates mechanical softening before failure. Other studies have investigated grain displacement at the free surface [7, 8], revealing intermittent behavior corresponding to bursts of collective displacements described by a complex distribution of event sizes, with small events following a power law. Larger recurrent events, called avalanche precursors, occur at well-defined increments of inclination  $\sim 1^\circ$  [7, 9, 10].

However, as demonstrated in [3] and [11], the dynamics preceding an avalanche are also rich within the bulk, enlightening the spatial distribution of local ruptures which density decrease with the depth. The grain-scale mechanisms responsible for large, intermittent plastic events—referred to as "micro-failures"—remain poorly understood. This paper investigates the kinematics of precursors to granular avalanches by measuring local strain fluctuations using two complementary techniques: Diffusive Acoustic Wave Spectroscopy (for the bulk) and grain imaging.

## 2 Experimental Setup

The experimental setup is shown in Figure 1(a). It consists of a transparent, smooth-bottomed rectangular container with a height of 20 cm, width of 50 cm, and thickness of  $13d$ , where  $d$  is the diameter of the grains. The container is filled with monodisperse spherical ceramic beads ( $d = 1.5 \pm 0.01$  mm) and water, and is mounted on a motorized rotating stage. To characterize the grain motion in the bulk using Diffusive Acoustic Wave Spectroscopy (DAWS), we send a pulse with a 1 MHz immersion transducer (diameter  $d_t = 13$  mm, Panametrics) and receive the signal with a small pinducer (diameter  $d_p = 1.5$  mm).

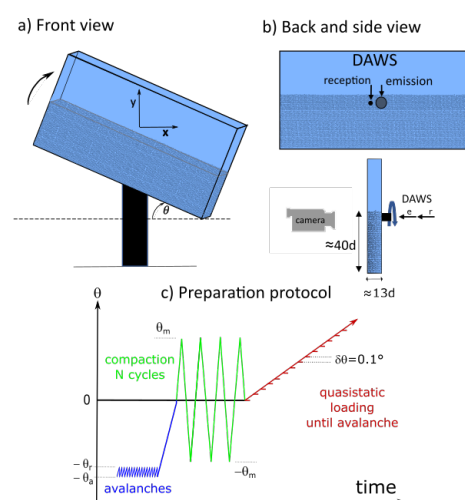


**Figure 1.** Experimental setup: (a) Sketch of the sample container, (b) Ultrasound emission and reception transducers and camera for recording the positions of the grains. (c) Protocol for preparing the granular samples.

The transducers are shown in Figure 1(b). Given the wavelength  $\lambda = 1.5$  mm, the waves are multiply scat-

\*e-mail: julien.leopoldes@univ-eiffel.fr

tered [12]. By averaging 100 signals propagated through different configurations, we obtain the coherent wave, which is then subtracted from each signal, leaving the multiply scattered part. These scattered signals from two granular configurations are then compared by computing the correlation function  $g_1$  [12] (see below).

In addition, a camera takes pictures of the grains on the container wall. By analyzing the images, we detect the grains and follow their trajectories. Using the grain positions at two different  $\theta$ , we determine the grain-scale strain field from the deformation of Delaunay triangles [13]. Next, we calculate a spatial average of the strains,  $\bar{\epsilon}$ , considering all the triangles included in a box of height  $12d$  and width  $16d$ , centered in the middle of the transducer positions. Finally, the strain is ensemble-averaged to obtain  $\langle \bar{\epsilon} \rangle$ . In the following, we focus on the shear strain  $\epsilon_{xy}$  and on the quadratic shear strain  $\epsilon_{xy}^2$ .

As shown in Figure 1(c), the granular packings are prepared with a protocol that first involves continuous rotation of the container above the avalanche angle  $\theta_a$ , allowing many avalanches to occur and erasing the memory of the previous configuration. Then, the system is oscillated  $N = 0, 1, 3$  or  $50$  times below the angle of repose at an angle  $\pm\theta_{osc} = 19.8^\circ$ , providing different states of compaction [14]. From the position of the free surface, the protocol yields different initial global packing fractions:  $\phi_0(N) = 0.608, 0.620, 0.623, 0.627$  for  $N = 0, 1, 3, 50$ , respectively.

The free surface is subsequently returned to horizontal. At this point, the container is inclined quasi-statically in steps of  $\delta\theta = 0.1^\circ$  until the angle of avalanche  $\theta_a$ , at which the granular flow occurs. At each step of the quasi-static loading, a picture of the grains and an acoustic signal are recorded.

### 3 Results

In the inset of Figure 2a, we plot the shear strain measured in a selection of individual experiments without a prior compaction cycle before shearing ( $N = 0$ ). The intensity of the shear strain increases as a function of  $\theta$ , until reaching approximately  $|\bar{\epsilon}_{xy}| \approx 5\%$  where the avalanche begins. It can be seen that each curve is composed of segments where no deformation occurs, interspersed with finite strain events.

Averaging the strain in the inset of the Figure 2(a) over intervals of  $\pm 1^\circ$  gives the red curve in the main panel of the Figure 2(a) ( $N = 0$ ). This curve can be compared to those for denser systems obtained with  $N = 1$  (blue),  $N = 3$  (green), and  $N = 50$  (magenta) compaction cycles. At a given  $\theta$ , the average strain is higher for lower initial packing fractions. Moreover, the angle of avalanche is higher for denser packings. As shown in Fig. 2(b), the shear strain is accompanied by a significant, albeit smaller, negative ensemble-averaged volumetric strain, indicating that some compaction occurs during shearing. Such volumetric strain occurs intermittently, synchronized with the finite shear strain events. Just before avalanching, all packings exhibit dilation. Typical relative displacements between grains in this study amount to about  $50\mu\text{m}$  [15].

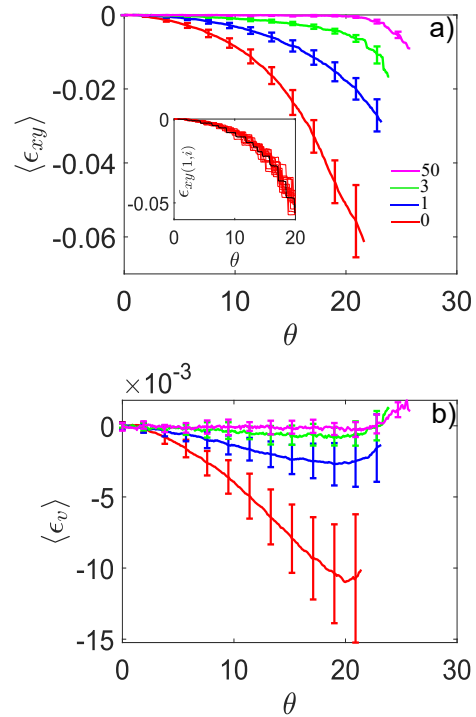


**Figure 2.** (a) Ensemble-averaged cumulative shear strain  $\langle \bar{\epsilon}_{xy} \rangle$  for  $N = 0$  (red),  $N = 1$  (blue),  $N = 3$  (green), and  $N = 50$  (magenta) compaction cycles. Inset: cumulative shear strain  $\bar{\epsilon}_{xy}$  shown for a selection of 20 different experiments for packings prepared without a prior compaction cycle before shearing ( $N = 0$ ). For illustrative purposes, the black curve highlights one arbitrary experimental result. (b) Ensemble-averaged cumulative volumetric strain. Same legend as in (a).

Throughout this study, we refer to finite strain events as "micro-failures".

We now plot in Figure 3(a) an example of two ultrasound signals  $\Psi$  taken before ( $\theta = 18.9^\circ$ ) and after ( $\theta = 19^\circ$ ) a micro-failure for the sample at  $N = 0$ . The modification of the signal is indicative of the relative motion of grains in 3D. The measured correlation function  $g_1 = \frac{\int \Psi_i \Psi_j dt}{(\int \Psi_i^2 dt \int \Psi_j^2 dt)^{1/2}}$  from such consecutive signals will be smaller than 1 (decorrelation) and can be linked to microscopic kinematics with the model by Cowan [12, 16], providing  $g_1 = \cos(n\langle \Delta\Phi \rangle) \times \exp\left(-\frac{n}{2}V\langle \Delta\Phi \rangle\right)$ . Here,  $\langle \Delta\Phi \rangle = \frac{1}{3}kl\langle \epsilon_v \rangle$ ,  $V\langle \Delta\Phi \rangle = \frac{2}{15}(kl)^2\langle \epsilon_{ws}^2 \rangle$  with  $\langle \epsilon_{ws}^2 \rangle = \langle \epsilon_v^2 \rangle + 2 \sum_{i,j} \langle \epsilon_{i,j}^2 \rangle$ .  $k = 2\pi/\lambda$  is the wave number and  $l \approx d$  is the mean free path. Note that in such a pulsed experiment, the decorrelation of acoustic signals is independent of boundary conditions [12]. With the propagation time  $t_s$ , the number of scattering event is  $n = t_s v/l \approx 25$  where  $v$  is the sound speed in water. Importantly, DAWS unveils micro-failures by capturing their signature in the quadratic strain field.

The evolution of  $g_1$  for consecutive signals separated by  $0.1^\circ$  is shown in Figure 3(b) (black) as a function of the tilt angle. The various downward spikes of  $g_1$  indicate micro-failures and are concomitant with upward spikes in quadratic shear strain (blue curve in Figure 3(b)). In the

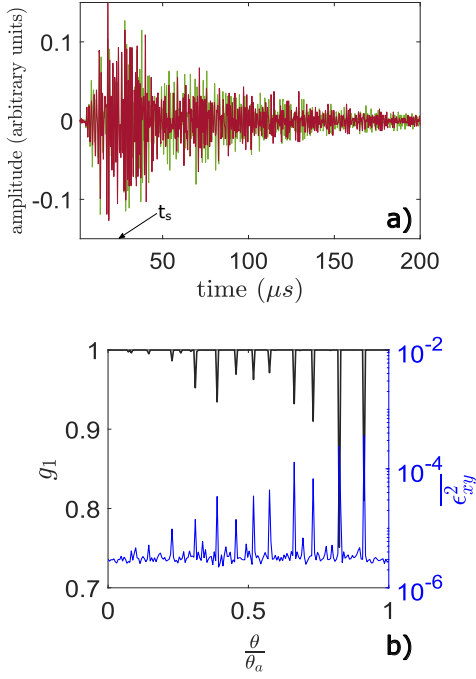


**Figure 3.** (a) Examples of raw signals. The brown and green signals correspond to before and after a precursor, respectively. The propagation time used for correlating the signals is  $t_s = 25 \mu s$  (b) Correlation function  $g_1$  of acoustic signals (black) and quadratic strain  $\overline{\epsilon_{xy}^2}$  for an experiment at  $N = 0$ .  $g_1$  and  $\overline{\epsilon_{xy}^2}$  are calculated over successive acquisitions, separated by an increment of inclination  $\Delta\theta = 0.1^\circ$ .

following, we focus on discrete events that simultaneously verify  $g_1 \leq 0,99$  and  $\overline{\epsilon_{xy}^2} \geq 1 \times 10^{-5}$ . These events, detected by both methods, are reliable signatures of micro-failures in the granular medium before avalanche.

Ensemble-averaged values of the quadratic strain obtained from DAWS during micro-failure events are presented alongside direct optical measurements of the single-component quadratic shear strain in Figure 4(a). The data are normalized by their maximum value reached at the last precursor before the avalanche begins, corresponding to  $\theta_m < \theta_a$ . The values of  $\theta_m$  are  $20.9 \pm 0.6$ ,  $22.8 \pm 0.7$ ,  $23.7 \pm 0.5$ , and  $24.8 \pm 0.9$  for  $N = 0, 1, 3, 50$  compaction cycles, respectively. All the data collapse onto a master curve that can be fitted with an exponential function of the form  $\frac{\langle \overline{\epsilon_{xy,ws}^2} \rangle}{\langle \overline{\epsilon_{xy,ws}^2} \rangle_m} = \exp \left[ A \left( \frac{\theta}{\theta_m} - 1 \right) \right]$  with parameter  $A \approx 4.8$ .

Furthermore, the fluctuations observed at the final (and largest) precursor event,  $\langle \overline{\epsilon_{xy}^2} \rangle_m$  and  $\langle \overline{\epsilon_{ws}^2} \rangle_m$ , are plotted in Figure 4(b) as a function of  $(\phi_0 - \phi_a)/\phi_a$ , the relative difference between the initial packing fraction  $\phi_0(N)$  and the packing fraction  $\phi_a \approx 0.603$  measured during flow when the granular media is a dense liquid, common to all packings.  $(\phi_0 - \phi_a)/\phi_a$  is used to quantify how far the initial state is from the dense liquid state. The maximum fluctuations decrease with  $\phi_0$ , and the data can be fitted with  $\langle \overline{\epsilon^2} \rangle_m = -B \times \frac{(\phi_0 - \phi_a)}{\phi_a} + C$ , with  $B_{ws} = 9.8 \times 10^{-2}$ ,  $B_{xy} =$

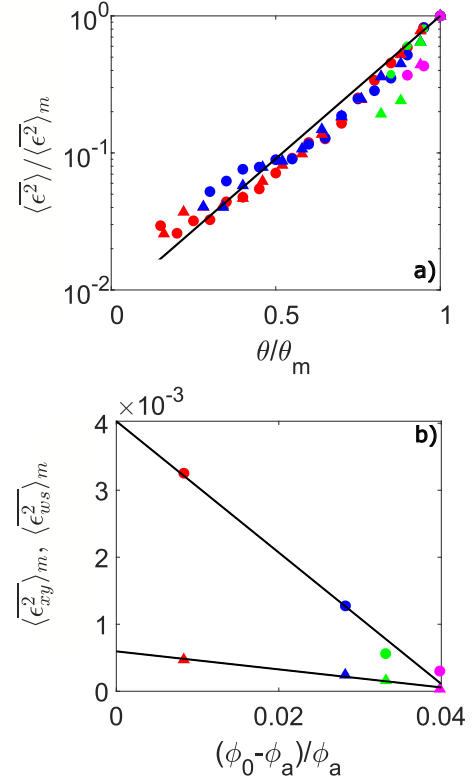


**Figure 4.** Quadratic strain of micro-failures  $\langle \overline{\epsilon^2} \rangle$  from DAWS and optical imaging (shear component), normalized by the maximum quadratic strain  $\langle \overline{\epsilon^2} \rangle_m$  at the last strain events before failure. Disks represent data from DAWS, and triangles represent data from optics. Colors correspond to  $N = 0$  (red),  $N = 1$  (blue),  $N = 3$  (green), and  $N = 50$  (magenta) compaction cycles. Plain line is an exponential fit (see text). (b) Quadratic strain  $\langle \overline{\epsilon_{xy}^2} \rangle_m$  and  $\langle \overline{\epsilon_{ws}^2} \rangle_m$  at the last precursor before large scale failure, as a function of the relative difference between the initial volume fraction  $\phi_0$  and the packing fraction during flow  $\phi_a \approx 0.603$ . Symbols correspond to the same conditions as in (a). Plain lines are linear fits (see text).

$1.4 \times 10^{-2}$  and  $C_{ws} = 4.1 \times 10^{-3}$ ,  $C_{xy} = 6.1 \times 10^{-4}$ . The results suggest that increased initial packing compactness leads to reduced quadratic strain from micro-failures, compared to states approaching the packing fraction of the dense liquid. With  $C/B \approx 4.6\%$  for acoustics and  $4.2\%$  for optics, the two independent methods suggest that once the packing fraction increases by a few percent above  $\phi_a$ , precursors are no longer detectable.

The plot in Figure 4(b) indicates that the ratio  $\langle \overline{\epsilon_{xy}^2} \rangle_m / \langle \overline{\epsilon_{ws}^2} \rangle_m \sim 0.1$ . Therefore, it is tempting to compare the two measurements more quantitatively. We measured optically  $\langle \overline{\epsilon_{xx}^2} \rangle$ ,  $\langle \overline{\epsilon_{yy}^2} \rangle$ ,  $\langle \overline{\epsilon_{xy}^2} \rangle$ , and  $\langle \overline{\epsilon_v^2} \rangle$  for every precursor and found that they are all the same order of magnitude. Assuming that the quadratic terms  $\langle \overline{\epsilon_{xz}^2} \rangle \approx \langle \overline{\epsilon_{yz}^2} \rangle \approx \langle \overline{\epsilon_{zz}^2} \rangle$  are small, we have, with  $i, j \neq z$ , an estimate of what is measured with ultrasound  $\langle \overline{\epsilon_{ws}^2} \rangle = (\langle \overline{\epsilon_v^2} \rangle + 2 \times \sum_{i,j} \langle \overline{\epsilon_{i,j}^2} \rangle) \approx 9 \langle \overline{\epsilon_{xy}^2} \rangle$ , in agreement with experimental data from optics. Hence, the model by [16] indicates that transverse quadratic strains can be neglected in our system. Note that

a comparison between the acoustic and optical methods can also be achieved by examining the mean square displacement of the grains. Both methods yield similar results [15].

## 4 Analysis and Discussion

The typical strain from micro-failures at the onset of the avalanche (see discrete events in the inset of the Figure 1(a) near 20°), correspond to  $\langle \overline{\epsilon_{xy}} \rangle_m \sim 10^{-2}$ , so from Figure 4(b), we have  $\langle \overline{\epsilon_{xy}^2} \rangle_m \sim 10^{-3} \gg \langle \overline{\epsilon_{xy}} \rangle_m^2$ . Therefore, the variance of the strain is essentially dominated by the quadratic strain, which represents a measure of strain fluctuations.

Our observations imply that the failure mechanisms in compact and loose packings are fundamentally different. In loose packings, large fluctuations indicate that the overall mean strain develops progressively through pronounced strain heterogeneities. These localized deformations may coalesce, potentially leading to the destabilization of the entire system. In contrast, the densest packings remain stable until a sudden, more catastrophic failure occurs, with little warning from micro-failures. While this phenomenology may be influenced by confinement effects in our setup (with a cell thickness  $L \approx 13d$ ), it is noteworthy that the vanishing amplitude of precursory events at high packing fractions was also observed in [17], where confinement effects are unlikely to play a significant role.

Spatial strain fluctuations serve as a useful proxy for monitoring the micro-failures that precede the main system-size catastrophic event. While the packing fraction appears to play an important role in the emergence of micro-failures, other structural parameters, such as the coordination number and fabric, shall be considered.

## 5 Conclusion

We have studied micro-failures in granular media by means of an experimental setup that combines optical tracking of the grains and DAWS. Both methods show that deformation fluctuations associated with avalanche precursors increase exponentially with the angle of inclination of the free surface. The maximum fluctuations measured at the onset of avalanche decrease with the initial packing fraction. Further work will include the study of the local mechanisms governing the strain fluctuations and their spatial correlations.

## References

- [1] B. Andreotti, Y. Forterre, O. Pouliquen, *Granular Media: Between Fluid and Solid* (Cambridge University Press, 2013)
- [2] H.M. Jaeger, S.R. Nagel, R.P. Behringer, *Granular solids, liquids, and gases*, *Rev. Mod. Phys.* **68**, 1259 (1996). [10.1103/RevModPhys.68.1259](https://doi.org/10.1103/RevModPhys.68.1259)
- [3] Kabla, A., Debrégeas, G., di Meglio, J.-M., Senden, T. J., X-ray observation of micro-failures in granular piles approaching an avalanche, *Europhys. Lett.* **71**, 932 (2005). [10.1209/epl/i2005-10165-4](https://doi.org/10.1209/epl/i2005-10165-4)
- [4] T.S. Majmudar, R.P. Behringer, Contact force measurements and stress-induced anisotropy in granular materials, *Nature* **435**, 1079 (2005). [10.1038/nature03805](https://doi.org/10.1038/nature03805)
- [5] F. Dalton, D. Corcoran, Self-organized criticality in a sheared granular stick-slip system, *Phys. Rev. E* **63**, 061312 (2001). [10.1103/PhysRevE.63.061312](https://doi.org/10.1103/PhysRevE.63.061312)
- [6] G. Mainsant, E. Larose, C. Brönnimann, D. Jongmans, C. Michoud, M. Jaboyedoff, Ambient seismic noise monitoring of a clay landslide: Toward failure prediction, *Journal of Geophysical Research: Earth Surface* **117** (2012). <https://doi.org/10.1029/2011JF002159>
- [7] N. Nerone, M.A. Aguirre, A. Calvo, D. Bideau, I. Ippolito, Instabilities in slowly driven granular packing, *Phys. Rev. E* **67**, 011302 (2003). [10.1103/PhysRevE.67.011302](https://doi.org/10.1103/PhysRevE.67.011302)
- [8] P. Richard, P. Philippe, F. Barbe, S. Bourlès, X. Thibault, D. Bideau, Analysis by x-ray microtomography of a granular packing undergoing compaction, *Phys. Rev. E* **68**, 020301 (2003). [10.1103/PhysRevE.68.020301](https://doi.org/10.1103/PhysRevE.68.020301)
- [9] S. Kiesgen de Richter, G. Le Caër, R. Delannay, Dynamics of rearrangements during inclination of granular packings: the avalanche precursor regime, *Journal of Statistical Mechanics: Theory and Experiment* **2012**, P04013 (2012). [10.1088/1742-5468/2012/04/P04013](https://doi.org/10.1088/1742-5468/2012/04/P04013)
- [10] L. Staron, F. Radjai, J.P. Vilotte, *Journal of Statistical Mechanics: Theory and Experiment* **2006**, P07014 (2006). [10.1088/1742-5468/2006/07/P07014](https://doi.org/10.1088/1742-5468/2006/07/P07014)
- [11] A. Amon, R. Bertoni, J. Crassous, Experimental investigation of plastic deformations before a granular avalanche, *Phys. Rev. E* **87**, 012204 (2013). [10.1103/PhysRevE.87.012204](https://doi.org/10.1103/PhysRevE.87.012204)
- [12] M.L. Cowan, I.P. Jones, J.H. Page, D.A. Weitz, Diffusing acoustic wave spectroscopy, *Phys. Rev. E* **65**, 066605 (2002). [10.1103/PhysRevE.65.066605](https://doi.org/10.1103/PhysRevE.65.066605)
- [13] K. Bagi, Stress and strain in granular assemblies, *Mechanics of Materials* **22**, 165 (1996). [https://doi.org/10.1016/0167-6636\(95\)00044-5](https://doi.org/10.1016/0167-6636(95)00044-5)
- [14] E.R. Nowak, J.B. Knight, E. Ben-Naim, H.M. Jaeger, S.R. Nagel, Density fluctuations in vibrated granular materials, *Phys. Rev. E* **57**, 1971 (1998). [10.1103/PhysRevE.57.1971](https://doi.org/10.1103/PhysRevE.57.1971)
- [15] I. Awada, M. Bornert, V. Langlois, J. Léopoldès, Fluctuations of local plastic strain in granular media, preprint arXiv:2503.17010 (2025).
- [16] D. Bico, R. Maynard, Diffusing wave spectroscopy in inhomogeneous flows, *Physica A: Statistical Mechanics and its Applications* **199**, 387 (1993). [https://doi.org/10.1016/0378-4371\(93\)90056-A](https://doi.org/10.1016/0378-4371(93)90056-A)
- [17] N. Gravish, D.I. Goldman, Effect of volume fraction on granular avalanche dynamics, *Phys. Rev. E* **90**, 032202 (2014). [10.1103/PhysRevE.90.032202](https://doi.org/10.1103/PhysRevE.90.032202)